Exp Fluids (2011) 50:839–846
DOI 10.1007/s00348-010-0928-7

RESEARCH ARTICLE

Full 3D correlation tensor computed from double field stereoscopic PIV in a high Reynolds number turbulent boundary layer

Jean-Marc Foucaut · Sebastien Coudert · Michel Stanislas · Joel Delville

Received: 4 January 2010 / Revised: 11 June 2010 / Accepted: 26 June 2010 / Published online: 15 July 2010

Abstract The turbulence structure near a wall is a very active subject of research and a key to the understanding and modeling of this flow. Many researchers have worked on this subject since the fifties Hama et al. (J Appl Phys 28:388–394, 1957). One way to study this organization consists of computing the spatial two-point correlations. Stanislas et al. (C R Acad Sci Paris 327(2b):55–61, 1999) and Kahler (Exp Fluids 36:114–130, 2004) showed that double spatial correlations can be computed from stereoscopic particle image velocimetry (SPIV) fields and can lead to a better understanding of the turbulent flow organization. The limitation is that the correlation is only computed in the PIV plane. The idea of the present paper is to propose a new method based on a specific stereoscopic PIV experiment that allows the computation of the full 3D spatial correlation tensor. The results obtained are validated by comparison with 2D computation from SPIV. They are in very good agreement with the results of Ganapthisubramani et al. (J Fluid Mech 524:57–80, 2005a).

J.-M. Foucaut (✉) · S. Coudert · M. Stanislas
Univ Lille Nord de France, 59000 Lille, France
e-mail: jean-marc.foucaut@ec-lille.fr

J.-M. Foucaut · M. Stanislas
ECLille, LML, 59650 Villeneuve d'Ascq, France

J.-M. Foucaut · S. Coudert · M. Stanislas
CNRS, UMR, 8107, 59650 Villeneuve d'Ascq, France

J. Delville
Départment Fluides, Institut Pprime,
CNRS, Univ. de Poitiers-ENSMA,
UPR 3346, Thermique, Combustion, CEAT,
43 rue de l'Aérodrome, 86036 Poitiers Cedex, France

1 Introduction

The structural organization of near wall turbulence has been the subject of intensive researches over the past 60 years. These studies are of importance in practical applications in order to develop realistic models at higher Reynolds numbers. From an experimental point of view, researchers have used different experimental approaches ranging from visualization to hot-wire anemometry and, more recently, particle image velocimetry (PIV). The initial purpose was to measure statistics of boundary layer turbulence. Klebanoff (1955) investigated the turbulent boundary layer using hot-wire anemometry. He gave many statistical results that contributed to the development and validation of turbulence models. For more than 20 years, many statistical properties of a wall-bounded flow have been well known and turbulent models have been derived from semi-empirical assumptions based on these results. In parallel, studies on the organization were performed to try to understand the auto-generation of turbulence in the near wall region. Based also on numerical simulation, different models of this organization have been published (see Adrian et al. 2000; Del Alamo et al. 2006, for examples).

A first approach to the organization study consists of computing the spatial and/or temporal two-point correlations. This approach has first been used with hot wire rake data using a Taylor hypothesis. The first investigation of this type was performed by Favre et al. (1957, 1958) and Tritton (1967) who studied the spatio-temporal structure of the streamwise velocity component by using a pair of spatially separated hot-wire probes. Kovasznay et al. (1970) used space–time correlation to study the external intermittency of the boundary layer. They proposed a 3D representation of the correlation reconstructed from their data. Their conclusion was that the burst phenomenon is

strongly 3-D. Moin and Kim (1985) computed spatial correlation from numerical simulation of a channel flow. They worked mainly on the existence of hairpin vortex inclined at 45°. They showed that the size of the structures increases with the wall distance. Some recent results from an experiment in turbulent boundary layer are presented in Tutkun et al. (2009). These results were obtained from a hot wire rake with multiple combs. In their paper, they discussed the influence of the large-scale motion on the turbulent flow using the space–time correlations.

Stanislas et al. (1999) showed that double spatial correlations computed from PIV fields allow a better understanding of the turbulent flow organization. They demonstrated the richness of such a tool when it is coupled with conditional sampling. Kahler (2004) characterized the structure size and organization of the buffer region of a turbulent boundary layer using such an approach, based on SPIV data. Ganapthisubramani et al. (2005a) investigated the large-scale organization using spatial correlations computed from velocity fields measured in different SPIV planes.

In the last 25 years, PIV has proved its capability and is now an accepted method to measure two components of the velocity in a plane (Adrian 1991; Westerweel 1997). Such a method allows spatial studies of turbulent flow and particularly of the near wall region (Stanislas et al. 2008). The stereoscopic PIV setup was a significant improvement for the study of complex flow. It allows the three components of the velocity field to be obtained in a plane by the use of two cameras (Willert 1997; Soloff et al. 1997). Usually, the cameras and lasers used have low repetition rates. This does not allow the temporal evolution of the flow to be resolved. One method used to overcome this limitation is the dual-plane PIV technique (Kähler and Kompenhans 2000). A double stereoscopic PIV system is used and the two light paths are separated by polarization. The dual-plane technique allows measurement of two velocity fields with an adjustable time delay or spatial separation between them. By varying this delay, the space–time correlation of the velocity field can be built. By varying the separation, the gradient tensor or the 3D spatial correlation can be built. Ganapthisubramani et al. (2005b) used the dual-plane technique to get the full gradient tensor and to study the near wall flow structure. Recently, Foucaut et al. (2009) showed the capability of High Repetition Stereoscopic PIV to obtain space–time correlation with very good resolution in a plane.

The objective of the present paper is to propose a new method to obtain the full 3D correlation tensor by taking advantage from the homogeneity of the flow. For that purpose, an original experiment to characterize the full turbulent boundary layer was performed in the frame of the WALLTURB European project. This experiment concerns the simultaneous measurement in two perpendicular SPIV planes (i.e. both planes are normal to the wall) in the LML wind tunnel Coudert et al. (2009). The first part of the present paper gives the details of the experiment and some results. The following part propose the original method of the 3D correlation tensor computation applied to the velocity fields of this experiment. The last part gives some results of correlation linked to the large-scale organization.

2 Experimental setup

The experiment was carried out in a turbulent boundary layer wind tunnel (Carlier and Stanislas 2005). The test section is 1 m high, 2 m width, and 20 m long to allow the development of the boundary layer. The last 5 m of the test section is transparent on all sides to allow the use of optical techniques. The wind tunnel works in a closed-loop configuration. The turbulent boundary layer is studied on the bottom wall of the wind tunnel test section. The Reynolds number, based on the momentum thickness R_θ, can reach 20,600 with a boundary layer thickness of about 0.3 m. The external velocity in the testing zone of the wind tunnel can vary from 0 to 10 m/s with a stability of 0.5%. The present experiment was carried out at two Reynolds number $R_\theta = 9{,}800$ and 19,800, which correspond to velocities of 5 and 10 m/s.

2.1 SPIV system

Figure 1 shows a top view of the setup. The x axis and z axis are in streamwise and spanwise directions, respectively. The y axis is normal to the wall. The first PIV plane (plane normal to the flow) is imaged with two Stereoscopic PIV systems in order to enlarge the field of view. Each

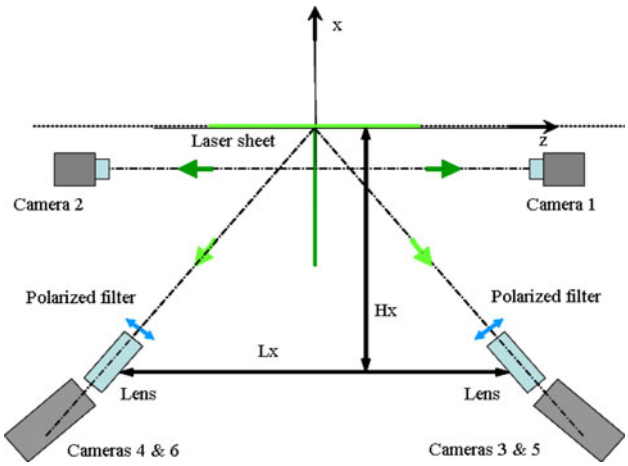

Fig. 1 Top view of the experimental setup

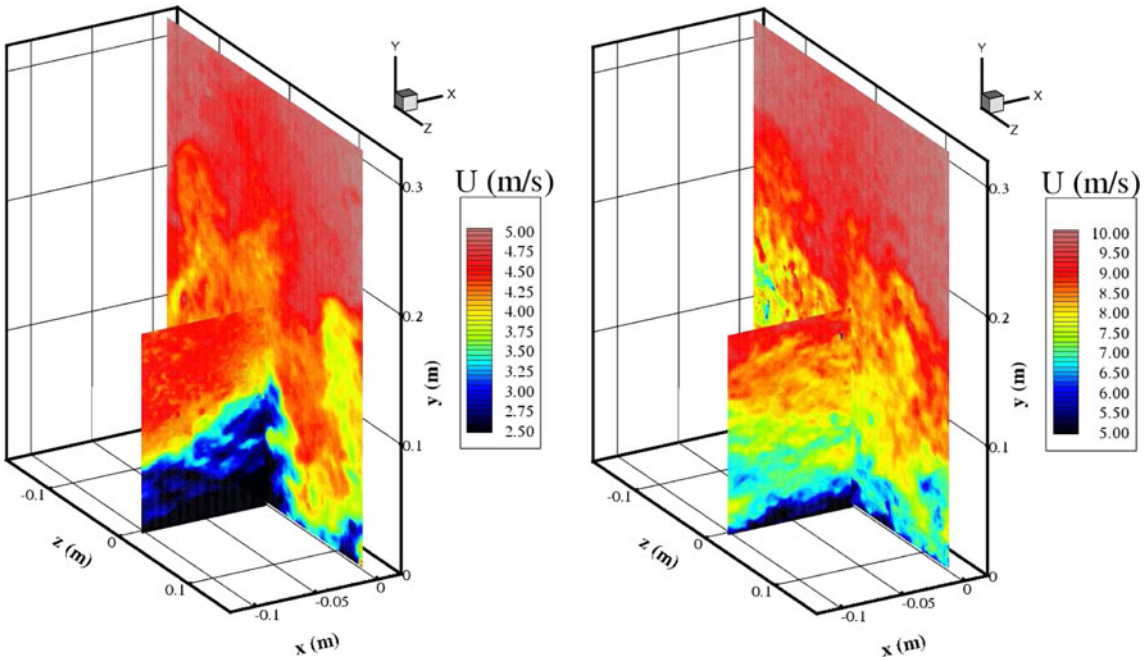

Fig. 2 Instantaneous streamwise velocity component, left-hand side $R_\theta = 9{,}800$ and right-hand side $R_\theta = 19{,}800$

system is based on Imager Intense cameras, from LaVision and a 50-mm lens. Both systems are adjusted with a small overlap region in order to obtain, after merging, a final field of view of about 30×32 cm^2. These dimensions are comparable to the boundary layer thickness. In that plane, the spatial resolution is 2 mm which corresponds to 50 wall units for the higher Reynolds number and about 25 wall units for the smallest. The second PIV field of view (plane parallel to the flow) is 10 cm long and 15 cm high. The system is composed of two PCO Sensicam cameras and two 100-mm lenses. The spatial resolution in this plane is 1 mm, which is half that of the previous plane. The laser used was a BMI YAG system with four cavities, which can deliver four beams two by two recombined and orthogonally polarized. Each camera lens was fitted with a polarizing filter; consequently, for each camera only the corresponding light sheet is recorded on the images as for the dual-plane technique. Moreover, each SPIV system was set in Scheimpflug conditions. A total of 9,600 velocity fields per Reynolds number were recorded. Figure 2, from Delville et al. (2009), gives an example of the instantaneous streamwise velocity component u in the two planes.

2.2 PIV analysis

The images from both cameras were processed with a standard multi-grid algorithm with discrete window offset. The analysis was made by the classical FFT-based cross-correlation method with integer shift of both windows. A 1-D Gaussian peak fitting algorithm was used for the sub-pixel displacement determination. The final interrogation window size was 30×42 pixels (corresponding to a real size of 6×6 mm^2) and 26×38 pixels (3×3 mm^2) respectively for the plane normal and parallel to the flow. The PIV analysis characteristics are given in Table 1. The wall units are deduced from hot wire results by the slope of the log law (Carlier and Stanislas 2005). The interrogation window size is too large to resolve the smallest scales. This is not an issue because the focus is on the large-scale motions in this experiment. The vector spacing corresponds to a 70% mean overlap.

Table 1 PIV analysis characteristics

Characteristics	Units	$R_\theta = 9{,}800$	$R_\theta = 19{,}800$
External velocity	m/s	5	10
Friction velocity	m/s	0.185	0.35
Spatial resolution YZ	mm	2	2
Spatial resolution YZ	wu[a]	25	50
Spatial resolution XY	mm	1	1
Spatial resolution XY	wu[a]	12	25
Interrogation window size YZ	mm	6	6
Interrogation window size YZ	wu[a]	75	150
Interrogation window size XY	mm	3	3
Interrogation window size XY	wu[a]	36	75

[a] Wall units

The Soloff (1997) method using three calibration planes was used to reconstruct the three velocity components in the plane of measurement. This was performed using the

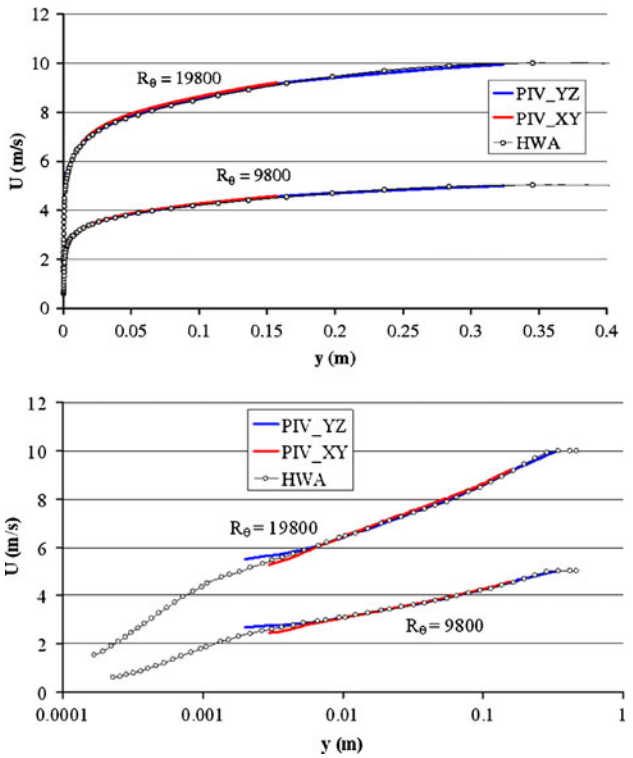

Fig. 3 Mean velocity profiles physical linear and semi-logarithmic representations

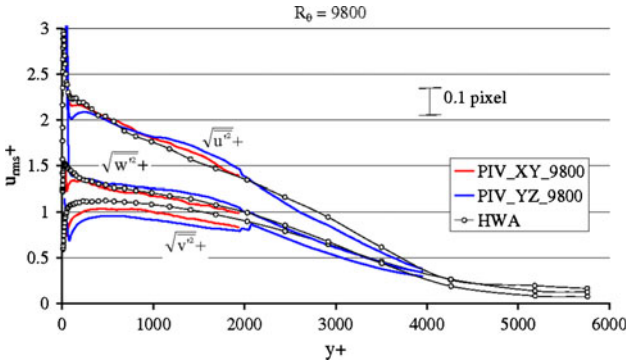

Fig. 4 Turbulence intensity profiles

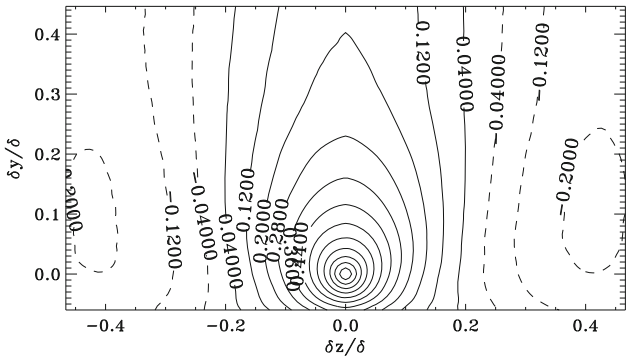

Fig. 5 2D correlation R_{11} in the YZ plane

PIVlml software developed at LML. The calibration was done with different targets using crosses. From the set of recorded calibration planes and SPIV images, the misalignment between the light sheet and the calibration plane was corrected (Coudert and Schon 2001).

2.3 PIV statistical results

Figure 3 show the mean streamwise velocity profiles in physical and semi-logarithmic representations for the two external velocities. In these figures, the velocities measured with the two PIV systems are in very good agreement with hot-wire anemometry data (HWA) published in Carlier and Stanislas (2005). Close to the wall, the PIV profiles separate from the HWA due to the mean velocity gradient inside the interrogation window.

For the lowest Reynolds number, Fig. 4 shows the profiles of standard deviation in wall units of the three velocity components for both PIV systems. The results are again in good agreement with the HWA data for both the spanwise and streamwise fluctuation profiles. The normal component seems slightly underestimated. The overlap region between the two fields of the YZ setup (measured by 2 SPIV systems) is located at $y+ = 2{,}000$. It allows an estimation of the accuracy from the discontinuity clearly visible on the fluctuation profiles. It is of the order of 0.04 m/s which corresponds to about 0.05 pixel.

3 Spatial correlation

The 2D and 3D correlations, proposed downstream, are computed for the lowest Reynolds number ($R_\theta = 9{,}800$).

3.1 2D correlations

From the above SPIV database, the double spatial correlations can be computed. The properties of these correlations are detailed in Stanislas et al. (1999) for standard PIV fields obtained in the same boundary layer and in a streamwise plane. It shows that the spatial correlation shape gives quantitative information about both shape and size of coherent structures. More recently, Kahler (2004) characterized some near wall coherent structures from Stereoscopic PIV. The use of SPIV allows the full correlation tensor to be obtained in a plane. As an example, R_{11} is shown in Fig. 5 for the lowest Reynolds number. The fixed point is at $y = 25$ mm corresponding to 0.08δ (i.e. 300 wall units). This correlation map corresponds to a standard turbulent boundary layer: a single peak is located at the fixed point. The size of the peak gives an indication on the size of the coherent region of the flow. This peak is about 0.2δ wide and 0.25δ high but extends well away from the wall. It is representative of the size of large-scale motion of

the boundary layer. Two negative peaks are located on each side of the main peak at about $\pm 0.4\delta$. This result is in good agreement with the results of Ganapathisubramani et al. (2006).

3.2 3D correlations

The new idea of the present paper is to propose a method to compute the 3D correlation tensor in the specific case of a 2D flow. To compute the 3D correlation, a volume measurement is necessary. However, if the flow is homogeneous along x and z direction, the 3D spatial correlation can be computed from the present experiment in the physical space. The streamwise direction can be taken as homogeneous direction because the field size along x is smaller than the thickness of the boundary layer. Using an approached law $\delta/x = 0.37Rex^{-0.2}$ (Schlichting 1979), it is easy to show that the variation of δ along x is of the order of 0.5% which is negligible. To compute the 3D correlations, the volume can be divided into two regions I and II as shown in Figs. 6 and 7 which are top views of the two planes. In region I (Fig. 6), the correlation can then be computed as:

$$R_{ij}(y,\delta x,\delta y,\delta z) = \frac{\overline{u_i^1(x_0-\delta x,y,0)u_j^2(x_0,y+\delta y,\delta z)}}{\sqrt{\overline{u_i^1u_i^1}}\sqrt{\overline{u_j^2u_j^2}}} \quad (1)$$

And in region II (Fig. 7) as:

$$R_{ij}(y,\delta x,\delta y,\delta z) = \frac{\overline{u_i^2(x_0,y,-\delta z)u_j^1(x_0+\delta x,y+\delta y,0)}}{\sqrt{\overline{u_i^1u_i^1}}\sqrt{\overline{u_j^2u_j^2}}} \quad (2)$$

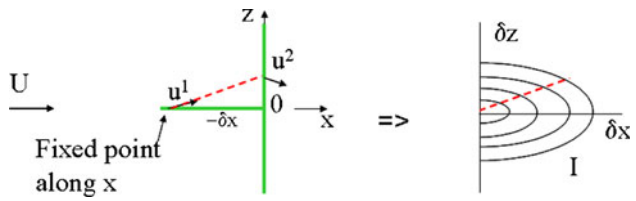

Fig. 6 Scheme of the method to compute the 3D correlation in the first half space

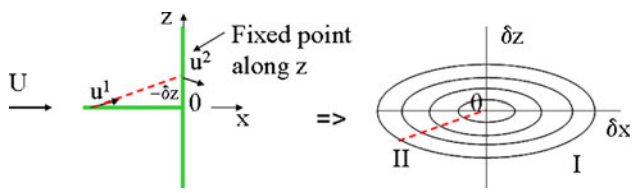

Fig. 7 Scheme of the method to compute the 3D correlation in the second half space

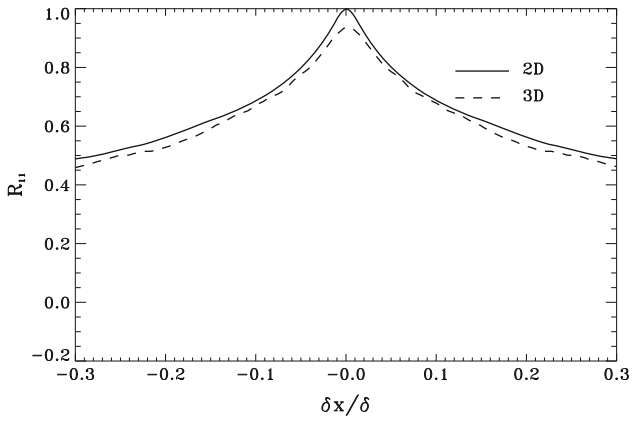

Fig. 8 Comparison of 2D and 3D correlation, XY plane

where $x = x_0$ and $z = 0$ are the coordinates of the two plane intersection, u_i^1 and u_i^2 are the normalized fluctuation components of the planes $z = 0$ and $x = x_0$, respectively, and the overbar corresponds to an average of the number of independent realizations which is about 10,000 in the present study.

As the mean flow is 2D, a symmetry condition can be imposed in order to double the convergence. The correlation R_{ij} must be symmetrical if $i = j$ or $i \neq j \neq 3$ in the other cases the correlation must be anti-symmetrical.

3.2.1 Comparison of 2D and 3D correlations

Figures 8 and 9 show a comparison of the 2D and 3D correlations as a cut along x and z in the case of a fixed point located at $y+ = 300$. As can be seen, both correlations are in quite good agreement. The global level of the 3D correlation is about 5% lower than the 2D one. This is due to the fact that this correlation is computed from two different PIV systems. The difference can be due to either the vector location errors of a plane with regard to the other or the measurement random error. Given the slope of the

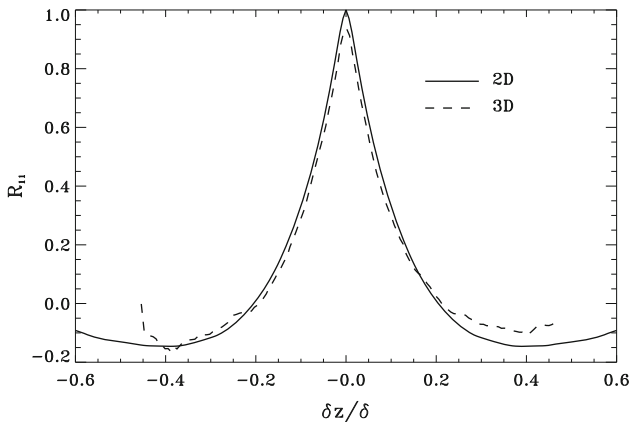

Fig. 9 Comparison of 2D and 3D correlation, YZ plane

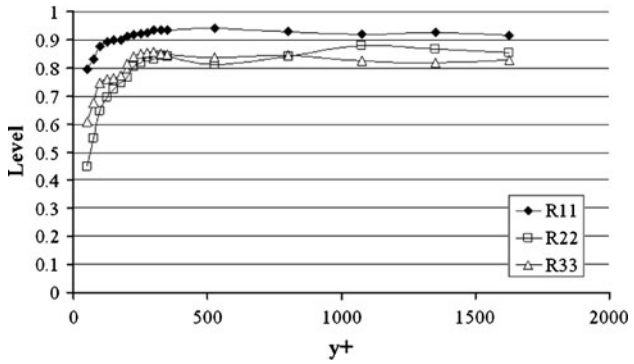

Fig. 10 Level of the 3D correlation R_{ii} at the fixed point versus the wall distance

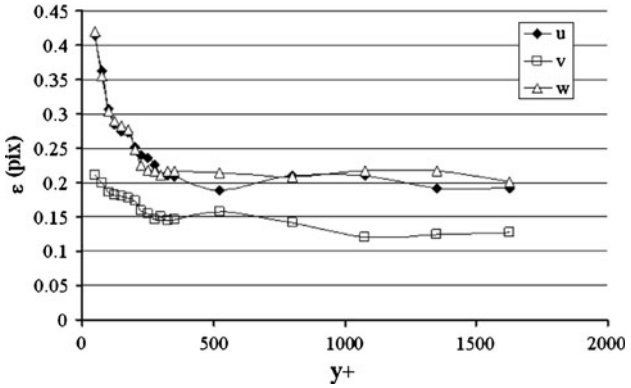

Fig. 11 RMS error estimation deduced from 3D correlation computation

correlation close to 0, the attenuation due to the difference in location is estimated of the order of 1–2%. The main difference is probably due to measurement errors. A correlation of 1 at $\delta_x = 0$, $\delta_y = 0$, and $\delta_z = 0$ would indicate a perfect measurement with no difference between both systems. The slightly lower level is due to errors of both PIV systems which do not correlate.

Figure 10 gives the level at the fixed point (for $\delta_x = 0$, $\delta_y = 0$, and $\delta_z = 0$) of each correlation R_{ii} versus the wall distance. The level of R_{11} is always higher than the other correlations. The levels are relatively constant expect close to the wall where they decrease with decreasing wall distance and thus when the mean velocity gradient increases. This result shows that the difference in the maximal level can be linked to the measurement error. Due to the fact that a large window size and no deformation were used in the PIV analysis, this error increases when the mean velocity gradient increases Foucaut et al. (2004). At about 300 wall units, the level seems to be constant at $R_{11} = 0.95$, $R_{22} = 0.84$, and $R_{33} = 0.85$.

Using the maximal value of the 3D correlation, an estimation of the measurement error can be done as:

$$\overline{\left(u_i^2(x_0,y,0) - u_i^1(x_0,y,0)\right)^2} = 2\overline{u_i u_i}\left(1 - R_{ii}(x_0,y,0)\right) \quad (3)$$

In this error estimation, the turbulent fluctuation levels measured in each PIV plane are considered to be the same $\overline{u_i u_i} = \overline{u_i^1 u_i^1} = \overline{u_i^2 u_i^2}$.

Figure 11 gives the estimations of the RMS error $\epsilon = \sqrt{\overline{\left(u_i^2(x_0,y,0) - u_i^1(x_0,y,0)\right)^2}}$ versus the wall distance in wall units. Far from the wall, the error is of the order of 0.2 pixel for the streamwise and spanwise component and 0.15 pixel for the wall normal component. As the location error is not taken into account, this error is probably slightly over-estimated, but it is coherent with the study of Foucaut et al. (2004). In the plane normal to the flow, which is the less accurate measurement, the wall normal component is not stretched by the stereoscopic setup. It gives then less

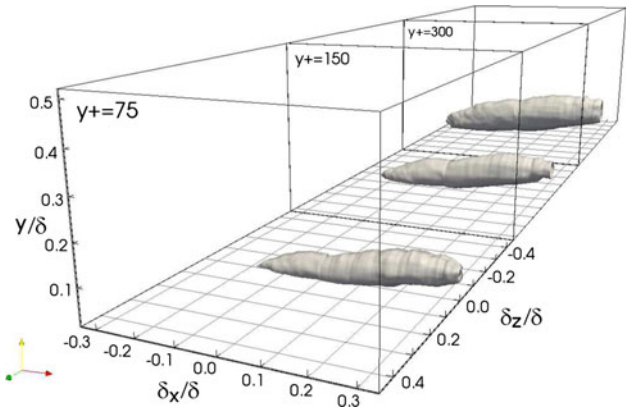

Fig. 12 Iso-contour at 0.5 of 3D correlation R_{11}, fixed points at y+ = 75, 150 and 300

filtering effect. This could probably explain the fact that the wall normal error estimation is lower.

In Figs. 8 and 9, a difference in convergence level can also be observed. In the 2D case, the homogeneity is used to increase the convergence (about a million samples), and in the 3D case the homogeneity is used to build the 3D (only about 10,000 samples). The lack of convergence is more critical when the correlation level decreases (for example when δz is far from 0).

3.2.2 3D correlation results

Figures 12, 13, 14, and 15 show the 3D isovalue of the correlations R_{11}, R_{22}, R_{33}, and R_{12} corresponding to a correlation level of 50% of the maximal value (minimal for R_{12} which presents a negative peak). Each figure shows the correlation computed for y+ = 75, 150, 300 in a box of $(0.6\delta; 0.5\delta; \delta)$. The friction velocity was taken in Carlier and Stanislas (2005).

R_{11} shows a very elongated region of correlation due to the streaky shape on the streamwise velocity component.

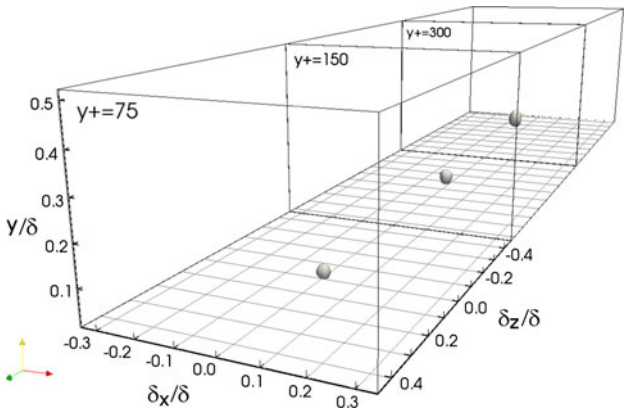

Fig. 13 Iso-contour at 0.5 of 3D correlation R_{22}, fixed points at y+= 75, 150 and 300

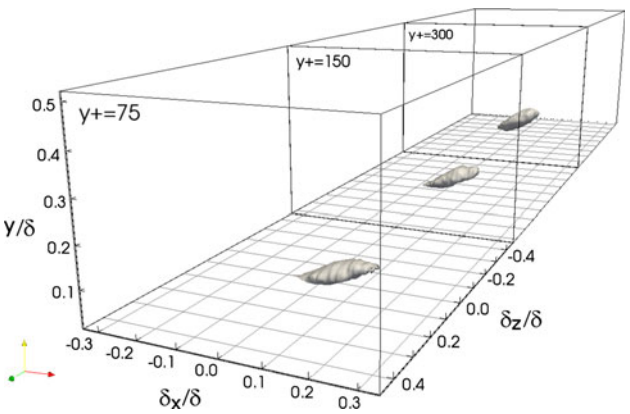

Fig. 14 Iso-contour at 0.5 of 3D correlation R_{33}, fixed points at y+ = 75, 150 and 300

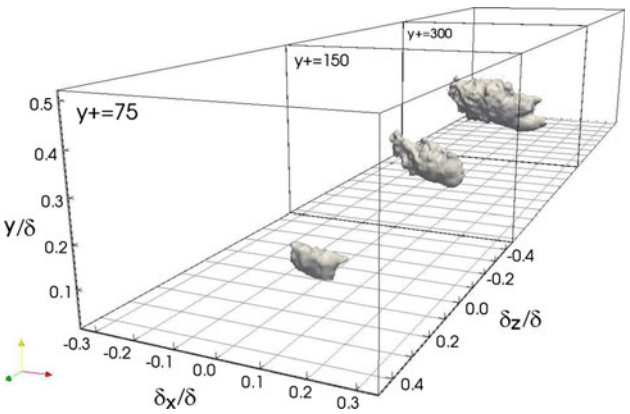

Fig. 15 Iso-contour at 0.5 of 3D correlation R_{12}, fixed points at y+ = 75, 150 and 300

This correlation looks like a long tube whose length increases with the wall distance from about 0.5δ to 0.7δ, and the maximal diameter increases from 0.1 to 0.2δ. This diameter is located at about 0.2δ downstream of the fixed point. This tube is inclined at an angle of almost 10° to the x-axis. Zhou et al. (1999) have obtained an angle from +10° to +15° from DNS computation which is in a good agreement with results from Kovasnay et al. (1970). These results support long coherence regions in the streamwise direction for this velocity component. The trend of the streamwise length is the same as Triton (1967). R_{22} looks like a sphere whose diameter increases from 0.04 to 0.06δ. The physical reason is not entirely obvious. The results for these two correlations are in very good agreement with Ganapthisubramani et al. (2005a).

R_{33} is also elongated in the streamwise direction but less than R_{11} and also more inclined. The length of R_{33} is of the order of 0.2δ. The shape of this correlation is not cylindrical but looks like an ellipsis in the plane YZ with a size of about 0.1δ by 0.06δ. This correlation seems less sensitive to the wall distance. Only the angle, which is about 30° close to the wall, tends to increase with the wall distance to about 45°. These results are in agreement with the hairpin vortex model inclined at 45° to the wall obtained by Moin and Kim (1985) in a channel flow and by Ganapthisubramani et al. (2005a) in a turbulent boundary layer.

Contrary to R_{33}, R_{12} is inclined in the upwind direction. The length of R_{12} increase with the distance of the fixed point from about 0.1δ to 0.3δ. The shape of this correlation is less regular than the other correlation probably due to a lack of convergence of this crossed correlation. At y+ = 150 wall units, the angle the angle of the correlation is very close to −45°. The shape of the correlation is mainly link to Sweep and Ejection. These results are in agreement with the results of Corrino and Brodkey (1969).

4 Conclusion

The computation of spatial correlations is a way to obtain quantitative information about the organization of a turbulent flow. The present paper proposes a new method to obtain the 3D correlation from a specific SPIV experiment in a turbulent boundary layer. Classically, SPIV gives velocity fields in a plane and only 2D correlation can be computed. A previously proposed solution is to record the velocity in two parallel planes using polarity of light to separate the two sheets (see Kahler 2004). The present idea is to make a single experiment in two orthogonal planes and to take advantage from the homogeneity of the flow along the streamwise and spanwise directions. This homogeneity allows building directly the 3D correlation as shown in Figs. 12, 13, 14, and 15. This data compare very well with the 2D correlation. At the intersection line of the two planes, an estimation of the measurement errors has been made using the value of the correlation. To obtain a good estimation of the correlation, both a huge number of

samples has to be recorded and the measurement quality must be very good.

The results obtained in the present paper are in very good agreement with the literature (i.e. Ganapthisubramani et al. 2005a). The 3D correlation allows obtaining new information on the shape of the coherent regions. For example, the maximal diameter of R_{11} is located at about 0.2δ downstream of the fixed point. Such a result cannot be obtained with only 2D cuts of the correlation tensor.

Acknowledgments The authors would like to acknowledge F. Benyoucef and D. Krolak who did a significant contribution to the development of the correlation computation software. This work has been performed under the WALLTURB project. WALLTURB (A European synergy for the assessment of wall turbulence) is funded by the CEC under the 6th framework program (CONTRACT No: AST4-CT-2005-516008). Part was also done in the frame of CISIT (International Campus on Safety and Intermodality in Transportation).

References

Adrian RJ (1991) Particle imaging techniques for experimental fluid mechanics. Ann Rev Fluid Mech 23:261–304

Adrian RJ, Meinhart CD, Tomkins CD (2000) Vortex organisation in the outer region of the turbulent boundary layer. J Fluid Mech 422(1)

Carlier J, Stanislas M (2005) Experimental study of eddy structures in a turbulent boundary layer using particle image velocimetry. J Fluid Mech 535:143–188

Corino ER, Brodkey RS (1969) A visual investigation of the wall region in turbulent flow. J Fluid Mech 37:1–30

Coudert S, Schon JP (2001) Back projection algorithm with misalignment corrections for 2D3C Stereoscopic PIV. Meas Sci Technol 12:1371–1381

Coudert S, Foucaut JM, Kostas J, Stanislas M, Braud P, Fourment C, Delville J, Tutkun M, Mehdi, Johansson P, George WK (2009) Double large field stereoscopic piv in a high reynolds number turbulent boundary layer. Exp Fluids. doi:10.1007/s00348-009-0800-9

Del Alamo JC, Jimenez J, Zandonade P, Moser RD (2006) Particle imaging techniques for experimental fluid mechanics. J Fluid Mech 561:329–358

Delville J, Braud P, Coudert S, Foucaut JM, Fourment C, George WK, Johansson P, Kostas J, Mehdi F, Royer A, Stanislas M, Tutkun M (2009) The wallturb joined experiment to assess the large scale structures in a high reynolds number turbulent boundary layer. In: Stanislas M, Jimenez J, Marusic I (eds) Workshop held in Lille. Springer ERCOFTAC Series

Favre A, Faviglio J, Dumas R (1957) Space-time double correlations and spectra in a turbulent boundary layer. J Fluid Mech 2:313–342

Favre A, Faviglio J, Dumas R (1958) Further space-time correlations of velocity in a turbulent boundary layer. J Fluid Mech 3:344–356

Foucaut JM, Miliat B, Perenne N, Stanislas M (2004) Characterization of different piv algorithms using the europiv synthetic image generator and real images from a turbulent boundary layer. In: Proceeding of the EUROPIV 2 Workshop on Particle Image Velocimetry, ed. Springer, pp 153–186

Foucaut JM, Coudert S, Stanislas M (2009) Unsteady characteristics of near-wall turbulence using high repetition stereoscopic particle image velocimetry (PIV). Meas Sci Technol 20. doi:10.1088/0957-0233/20/7/074004

Ganapathisubramani B, Hutchins N, Hambleton WT, Longmire EK, Marusic I (2005a) Investigation of large-scale coherence in a turbulent boundary layer using two-point correlations. J Fluid Mech 524:57–80

Ganapathisubramani B, Longmire EK, Marusic I, Pothos S (2005b) Dual-plane piv technique to determine the complete velocity gradient tensor in a turbulent boundary layer. Exp Fluids 39:222–231

Ganapathisubramani B, Longmire EK, Marusic I (2006) Experimental investigation of vortex properties in a turbulent boundary layer. Phys Fluids 18(055105.114)

Hama FR, Long JD, Hegarty JC (1957) On transition from laminar to turbulent flow. J Appl Phys 28:388–394

Kahler CJ (2004) Investigation of the spatio-temporal flow structure in the buffer region of a turbulent boundary layer by means of multiplane stereo PIV. Exp Fluids 36:114–130

Kahler CJ, Kompenhans J (2000) Fundamentals of multiple plane stereo PIV. Exp Fluids Suppl S70–S77

Klebanoff PS (1955) Characteristics of turbulence in a boundary layer with zero pressure gradient. NACA Report 1247

Kovasznay LSG, Kibens V, Blackwelder RF (1970) Large-scale motion in the intermittent region of the boundary layer. J Fluid Mech 41:283–325

Moin P, Kim J (1985) The structure of the vorticity field in turbulent channel flow. Part 1. Analysis of instantaneous fields and statistical correlation. J Fluid Mech 155:441–464

Schlichting H (1979) Boundary layer theory. McGraw-Hill, New York

Soloff S, Adrian R, Liu ZC (1997) Distortion compensation for generalized stereoscopic particle image velocimetry. Meas Sci Technol 8:1441–1454

Stanislas M, Carlier J, Foucaut JM, Dupont P (1999) Double spatial correlations, a new experimental insight into wall turbulence. C R Acad Sci Paris 327(2):55–61

Stanislas M, Perret L, Foucaut JM (2008) Vortical structures in the turbulent boundary layer: a possible route to a universal representation. J Fluid Mech 602:327–382

Tritton DJ (1967) Some new correlation measurements in a turbulent boundary layer. J Fluid Mech 28:439–462

Tutkun M, George W, Delville J, Stanislas, Johansson PM, Foucaut JM, Coudert S (2009) Two-point correlations in high reynolds number flat plate turbulent boundary layers 10:1–23

Westerweel J (1997) Fundamentals of digital particle image velocimetry. Meas Sci Technol 8(12):1379–1392

Willert C (1997) Stereoscopic digital particle image velocimetry for applications in wind tunnel flows. Meas Sci Technol 8:1465–1479

Zhou J, Adrian RJ, Balachandar S, Kendall TM (1999) Mechanism for generating coherent packets of hairpin vortices in channel flow. J Fluid Mech 387:353–396